Heat Transfer Enhancement of EMHD GO-MoS_2-Ag/H_2O Flow Toward Shrinking Riga Plate with Velocity and Thermal Slips Impacts

Nor Ain Azeany Mohd Nasir[1, 2, a)], Nooraini Zainuddin[3, b)], Norihan Md Arifin[2, 4, c)], Nur Syahirah Wahid[4, d)] and Ioan Pop[5, e)]

[1]*Department of Mathematics, Centre for Defence Foundation Studies, Universiti Pertahanan Nasional Malaysia, Kem Sungai Besi 57000 Kuala Lumpur, Malaysia.*
[2] *Laboratory of Computational Sciences and Mathematical Physics, Institute for Mathematical Research, Universiti Putra Malaysia, 43400 UPM Serdang, Selangor, Malaysia.*
[3]*Department of Fundamental and Applied Sciences, Faculty of Science and Information Technology, Universiti Teknologi PETRONAS, 32610 Seri Iskandar, Perak, Malaysia.*
[4]*Department of Mathematics and Statistics, Faculty of Science, Universiti Putra Malaysia, 43400 UPM Serdang, Selangor, Malaysia.*
[5]*Department of Mathematics, Babes-Bolyai University, 400084 Cluj-Napoca, Romania.*

[a)] Corresponding author: norainazeany@upm.edu.my
[b)] aini_zainuddin@utp.edu.my
[c)] norihana@upm.edu.my
[d)] syahirahwahid@upm.edu.my
[e)] popm.ioan@yahoo.co.uk

Abstract. The problem of heat transportation and ternary hybrid nanofluid flow over a shrinking Riga plate, as well as the effects of non-uniform heat source/sink, velocity, and thermal slip, is investigated. The nanometals used in this research for the ternary hybrid nanofluid are graphene oxide (GO), Molybdenum Sulfide (MoS_2) and silver (Ag) with fluid-based water (H_2O). The governing equations also involved electromagnetohydrodynamic (EMHD) combined with an electromagnetic surface named Riga plate, which are derived and further reduced to ordinary differential equations to reduce the complexity of the solution. The solutions are computed using a user-friendly solver, bvp4c, built-in MATLAB software. The findings indicate that velocity slip, Eckert number and magnetic parameter have similar effects toward the augmentation of temperature profiles and Nusselt number. However, the EMHD parameter forces the velocity, skin friction and Nusselt number to be diminished. Furthermore, the concentration of GO has a significant impact towards temperature profile, skin friction and Nusselt number to amplify. These findings benefit the process of advanced cooling systems, power converters and inverters for renewable energy, electric cars and many more.

INTRODUCTION

Recently, ternary hybrid nanofluid has collected significant amounts of consideration in research because of the enhancement of thermal prospect compared to hybrid nanofluid. The ternary hybrid nanofluid involved three nanoparticles which is extended of the concept of hybrid nanofluid. It is believed that ternary hybrid nanofluid can offered richer potential in optimising the thermal properties. However, the combination of ternary hybrid nanofluid with Riga plates is trusted to maximising the heat transferal competency. Riga plate served as fluid flow controller which efficiently manipulate the heat transferal and also known as electromagnetohydrodynamics (EMHD). Latest study on this particular topic from Nasir et al. [1] reported that the ternary hybrid nanofluid perform important act to improve the thermal efficiency with the effect of Riga plate. Followed by Abbas et al. [2] investigated the Darcy Forchheimer with ternary hybrid nanofluid towards Riga plate and they found out that the temperature profile augmented as thermal and heat source parameters amplified. Several researchers have

been investigating the ternary hybrid nanofluid flow with Riga plate such as Sajid et al. [3] which consider Hamilton and Crosser model with catalytic reaction and Jakeer et al. [4] which consider non-linear Darcy-Forchheimer with couple stress, to name a few.

In modern applications of fluid flow and heat transferal, the assumption of non-slip boundary conditions is obsoleted particularly when complex thermophysical fluid flow. The velocity slip is noted as differences velocity of the fluid with surface's velocity while thermal slip is defined as the difference of temperature gradient at boundary and adjacent fluid. Afridi et al. [5] investigated the slip effect towards AIN-Al2O3 Casson hybrid nanofluid and found that the slip affected the skin friction to diminish more than classical nanofluid. Moreover, the magnetohydrodynamic (MHD) Carreau fluid flow with the effect of thermal slip has been investigated by Ur Rehman et al. [6]. It is mentioned that the temperature profile fluctuated as the thermal slip augmented. It is interesting to study the impact of velocity and thermal slip as they can contribute to control the flow and heat. Other researchers that have been studied these impacts are Thumma and Mishra [7], Khan et al. [8], Al Arni et al. [9] and Mahmood et al. [10].

Based on the above literature, there are a lot of gaps to fill in especially involving ternary hybrid nanofluid and Riga plate. Hence, this study is aimed to model a mathematical modelling the flow of EMHD ternary hybrid nanofluid flow and heat transferal towards shrinking Riga plate with several impacts. The nanoparticles that involved in this study are GO, Molybdenum Sulfide (MoS_2) and silver (Ag) with fluid-based water (H_2O). The effects that being considered in this study are EMHD, concentration of GO, non-uniform heat source/sink, velocity and thermal slips. The mathematical model is then being reduced to ordinary differential equations (ODEs) to reduce the complexity of solving the model. The solutions of the model are computed by implementing bvp4c, a solver build in MATLAB software. The stability analysis of the solution is opted out due to the model is similar to Supian et al. [11] and Aminuddin et al. [12]. They both have already shown that the first solution is stable, and the second solution is unstable with no physical reason, thus the discussion will speculate on first solution but the second solution also being represented in the results.

MATHEMATICAL MODELING

The flow consists of GO, MoS_2 and Ag nanoparticles with based water along flat shrinking magnetic surface called Riga plate with the impact of non-uniform heat source/sink, velocity and thermal slip as depicted in Fig. 1. The x-axis is measured horizontally while the y-axis is acting perpendicular to the Riga plate. The velocity with stretching/shrinking surface noted as $u_w = ax$ and the mass velocity known as $v_w = v_0$ as well as the far field velocity as $u_e = ax$. The wall temperature denoted as T_w and the far field temperature is T_∞.

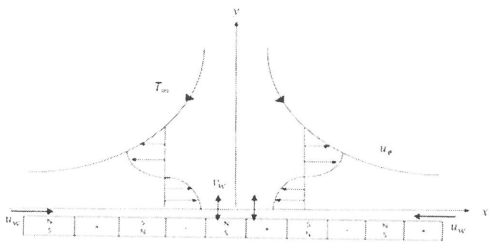

FIGURE 1. Schematic diagram of fluid flow over shrinking Riga plate.

Under these circumstances, the associated governing equations is given as (refs. Sufian et al. [11] and Aminuddin et al. [12]):

$$\frac{\partial u}{\partial x} + \frac{\partial v}{\partial y} = 0, \tag{1}$$

$$u\frac{\partial u}{\partial x} + v\frac{\partial u}{\partial y} = u_e\frac{\partial u_e}{\partial x} + \nu_{thnf}\frac{\partial^2 u}{\partial y^2} + \frac{\pi j_0 m_0 x}{8\rho_{thnf}}e^{-\frac{\pi y}{\omega}}, \tag{2}$$

$$u\frac{\partial T}{\partial x} + v\frac{\partial T}{\partial y} = \frac{k_{thnf}}{(\rho C_p)_{thnf}}\left(\frac{\partial^2 T}{\partial y^2}\right) + \frac{Q'''}{(\rho C_p)_{thnf}} - \frac{1}{(\rho C_p)_{thnf}}\left(\frac{\partial}{\partial y}\left[-\frac{16\sigma^* T_\infty^3}{3k^*}\left(\frac{\partial T}{\partial y}\right)\right]\right), \tag{3}$$

tagging along with unique boundary conditions,

$$\begin{aligned} u = \alpha u_w + \epsilon\frac{\partial u}{\partial y}, \quad v = v_0, \quad T = T_w + D\frac{\partial T}{\partial y} \quad at\ y = 0, \\ u \to u_e, \quad T \to T_\infty \quad as\ y \to \infty. \end{aligned} \tag{4}$$

The u and v noted as the velocity in x and y direction (axes), while $\nu, j_0, m_0, \rho, \omega, k, C_p, Q''', \sigma^*, k^*, \epsilon$ and D are defined as kinematic viscosity, current density in the electrodes, permanent magnetisation, density, electrodes thickness, thermal conductivity, specific heat, non-uniform heat source/sink, Stefan-Boltzmann constant, mean absorption, velocity and thermal slip respectively. The stretching and shrinking parameter noted as $\alpha > 0$ and$\alpha < 0$ while the injection and suction parameters known as $v_0 > 0$ and $v_0 < 0$ concurrently.

It is worth noting that the non-uniform heat source/sink is given by (ref. Abo-Eldahab et al. [13]),

$$Q''' = \frac{k_{thnf} u_w}{x \nu_{thnf}} [a(T_w - T_\infty)e^{-\eta} + b(T - T_\infty)]. \tag{5}$$

Given that a and b are the space and temperature dependencies internal heat source/sink. $a(T_w - T_\infty)e^{-\eta}$ denoted as the internal heat source/sink on the space points dependency and $b(T - T_\infty)$ refer to temperature dependency. The internal heat source is happening when $a, b > 0$ while $a, b < 0$ happened for internal heat sink.

By substituting (5) into (3), the energy equation becomes,

$$u\frac{\partial T}{\partial x} + v\frac{\partial T}{\partial y} = \frac{k_{thnf}}{(\rho C_p)_{thnf}}\left(\frac{\partial^2 T}{\partial y^2}\right) + \frac{1}{(\rho C_p)_{thnf}}\frac{k_{thnf} u_w}{x \nu_{thnf}} [a(T_w - T_\infty)e^{-\eta} + b(T - T_\infty)] - \frac{1}{(\rho C_p)_{thnf}}\left(\frac{\partial q_r}{\partial y}\right). \tag{6}$$

It is wise to reduce the governing equations (1), (2), (4) and (6) into ODEs for lessen the complexity of the solution computation. The similarity transformation is the easiest method for these purposes. The associated similarity variable that will be used in this study given by (ref. Aminuddin et al. [12])

$$\psi = \sqrt{u_0 v_f}\, x\, f \quad , \quad \eta = y\sqrt{\frac{u_0}{v_f}} \quad , \quad T = \theta(T_w - T_f) + T_f. \tag{7}$$

The streamlines ψ which is subject to the velocity as $u = \frac{\partial \psi}{\partial y}$ and $v = -\frac{\partial \psi}{\partial x}$ along x-axis. Hence, the governing equations (1), (2), (4) and (6) will reduced to

$$\varepsilon_1 \varepsilon_2 f''' + f f'' - f'^2 + 1 + R\varepsilon_2 e^{-\delta\eta} = 0, \tag{8}$$

$$\frac{1}{Pr\varepsilon_4}\left[(\varepsilon_3 + K)\theta'' + \frac{\varepsilon_3}{\varepsilon_1 \varepsilon_2}[ae^{-\eta} + b\theta]\right] + f\theta' = 0, \tag{9}$$

with reduced boundary conditions

$$f' = \alpha + \beta f'', \quad f = S, \quad \theta = 1 + \gamma\theta' \quad at\ y = 0$$
$$f' \to 1, \quad \theta \to 0 \quad as\ y \to \infty. \tag{10}$$

The associated non-dimensionless parameters in equation (8)-(10) is defined as nanofluid parameters, Riga plate width, radiation, thermal slip, EMHD, Prandtl number, velocity slip and suction/injection parameter respectively as follows:

$$\varepsilon_1 = \frac{\mu_{thnf}}{\mu_f}, \varepsilon_2 = \frac{\rho_f}{\rho_{thnf}}, \varepsilon_3 = \frac{k_{thnf}}{k_f}, \varepsilon_4 = \frac{(\rho C_p)_{thnf}}{(\rho C_p)_f}, \delta = \frac{\pi\sqrt{\frac{v_f}{u_0}}}{\omega}, K = \frac{16\sigma^* T_f^3}{3k^* k_f}, \gamma = D\sqrt{\frac{u_0}{v_f}}, R = \frac{\pi j_0 m_0}{8u_0^2 \rho_f}, Pr\ Pr = \frac{\mu_f (C_p)_f}{k_f}, \beta = \epsilon\sqrt{\frac{u_0}{v_f}}, S = \frac{-v_0}{\sqrt{u_0 v_f}}. \tag{11}$$

Since this study involved nanofluid parameters, there are needs to be shown the thermophysical properties of ternary hybrid nanofluid chosen as illustrated in Table 1. The volume concentration for ternary hybrid nano particles is denoted as φ_1 for graphene oxide (GO), φ_2 as Molybdenum disulphide (MoS_2) and φ_3 known as silver (Ag) while the based fluid is water (H_2O). The subscript hnf, nf and f refers as hybrid nanofluid, nanofluid and based fluid respectively.

TABLE 1. Thermophysical properties of ternary hybrid nanofluids. (Ref. Mumtaz et al. [14])

Properties	Ternary Hybrid Nanofluid Formula
Density	$\frac{\rho_{thnf}}{\rho_f} = (1-\varphi_3)\left[(1-\varphi_2)\left\{(1-\varphi_1)+\varphi_1\frac{\rho_{s1}}{\rho_f}\right\}+\varphi_2\frac{\rho_{s2}}{\rho_f}\right]+\varphi_3\frac{\rho_{s3}}{\rho_f}$
Dynamic viscosity	$\frac{\mu_{thnf}}{\mu_f} = \frac{1}{(1-\varphi_1)^{2.5}(1-\varphi_2)^{2.5}(1-\varphi_3)^{2.5}}$
Heat capacity	$\frac{(\rho C_p)_{thnf}}{(\rho C_p)_f} = (1-\varphi_3)\left[(1-\varphi_2)\left\{(1-\varphi_1)+\varphi_1\frac{(\rho C_p)_{s1}}{(\rho C_p)_f}\right\}+\varphi_2\frac{(\rho C_p)_{s2}}{(\rho C_p)_f}\right]+\varphi_3\frac{(\rho C_p)_{s3}}{(\rho C_p)_f}$
Thermal conductivity	$\frac{k_{thnf}}{k_f} = \left[\frac{k_{s3}+2k_{hnf}-2(k_{hnf}-k_{s3})\varphi_3}{k_{s3}+2k_{hnf}+(k_{hnf}-k_{s3})\varphi_3}\right]\left(\frac{k_{hnf}}{k_f}\right)$ where $\frac{k_{hnf}}{k_{nf}} = \frac{k_{s2}+2k_{nf}-2(k_{nf}-k_{s2})\varphi_2}{k_{s2}+2k_{nf}+(k_{nf}-k_{s2})\varphi_2}$ and $\frac{k_{nf}}{k_f} = \frac{k_{s1}+2k_f-2(k_f-k_{s1})\varphi_1}{k_{s1}+2k_f+(k_f-k_{s1})\varphi_1}$

It is also important to know the value of the thermophysical for each of the nanoparticles used in this study. The values of each thermophysical nanoparticles used is depicted in Table 2.

TABLE 2 The values of thermophysical ternary hybrid nanoparticles used in this study. (Refs. Aminuddin et al [12], Zainuddin et al. [15] and Nasir et al. [16])

Thermophysical properties	GO	MoS_2	Ag	H_2O
Thermal conductivity $k\ (Wm^{-1}K^{-1})$	5000	34.5	429	0.613
Density $\rho\ (kgm^{-2})$	1800	5060	10500	997.1
Specific heat $C_p(Jkg^{-1}K^{-1})$	717	397.746	235	4179
Dynamic viscosity $\mu\ (kgm^{-1}s^{-1})$	-	-	-	0.000855

The recognised physical quantities for equations (8)-(10) are known as skin friction coefficient and Nusselt number as follows (ref. Sufian et al [11]).

$$\text{Skin friction, } C_f = \frac{\mu_{thnf}}{\rho_f u_w{}^2}\left(\frac{\partial u}{\partial y}\right)_{y=0}, \text{ and Nusselt number, } Nu_x = -\frac{x k_{thnf}}{k_f(T_w-T_\infty)}\left(\frac{\partial T}{\partial y}\right)_{y=0}. \tag{12}$$

Substituting similarity variables (7) into equation (11) will be produced,

$$Re^{1/2}{}_x\, C_f = \varepsilon_1 f''(0), \text{ and } Re_x{}^{-1/2}\, Nu_x = -(\varepsilon_3 + K)\theta'(0), \tag{13}$$

where Reynolds number known as $Re_x = \frac{x u_w k_f}{(\rho C_p)_f}$.

RESULT AND DISCUSSIONS

The reduced ODEs (8)-(10) are then solved using bvp4c solver which is a solver package available in MATLAB software. The numerical computation solution is validated using a simplest method by comparing with previous published results available in the literature. The current computation solution is being compared with

solution reported by Swain et al. [17] and Arani and Aberoumand [18]. Swain et al. [17] computed the solution using the Broyden method coupling with RK4 for shooting technique. While Arani and Aberoumand [18] adapting Keller Box technique to compute their solutions. Table 3 illustrated the values of those computed solution with published results, and it can be concluded that the current computation results are reliable because of they agreeable with each other.

TABLE 3. Comparison between numerical computation of $f''(0)$ with varies α when $R = \delta = \beta = S = 0$ and $\varepsilon_1 = \varepsilon_2 = 1$. ([] is second solution).

α	Swain et al. [17]	Arani and Aberoumand [18]	Current results
-1.24657	0.574516, [0.564012]	-	0.574518739, [0.564013060]
-1.2465	0.584278, [0.554296]	-	0.584278991, [0.554296361]
-1.2	0.932473, [0.233650]	0.9324, [0.2336]	0.932473006, [0.233649671]
-1.18	-	1.0005, [0.1782]	1.000449103, [0.178361240]
-1.15	1.082231, [0.116702]	1.0824, [0.1169]	1.082231132, [0.116702094]
-1.1	-	1.1869, [0.0501]	1.186680250, [0.049228940]
-1	1.328816	-	1.328816861, [0.0]
-0.75	1.489298	-	1.489298211
-0.5	1.495669	-	1.495669739
-0.25	1.402240	-	1.402240795

Skin Friction and Nusselt Number

The skin friction is affected by GO concentration, EMHD and velocity slip parameters based on Table 4. It is eye-catching that the increment of GO concentrations will increase the skin friction. This phenomenon happened due to the GO nanoparticles will attribute to enhance surface roughness and electrostatic interaction which can affect the fluid flow. The augmentation of skin friction is further enhanced due to the Lorentz force produced by EMHD parameter. The force created the drag impact towards the nanoparticles which amplified the resistance to the flow. It is noted that the velocity slip declined the skin friction as the difference between fluid velocity and the surface is less pronounced.

Whilst, the GO concentration, EMHD, non-uniform heat source, velocity and thermal slip parameters have been affected the Nusselt number greatly. The viscosity of the fluid affected as GO nanoparticles increases in the flow which can minimised the ability of the fluid to transport the heat, hence the Nusselt number will decrease. It is widely known that the Lorentz force will diminish the thickness of the thermal boundary layer thus it impacts to augment the Nusselt number. The Nusselt number is further increased as the velocity slip influences the temperature gradient near the Riga plate. However, the thermal slip causing the heat flux to diminish which resulting further lowering the Nusselt number. It is also possible that the non-uniform heat sources to decline the Nusselt number by disrupting the thermal boundary layer leads to temperature fluctuations and instabilities.

TABLE 4. The values of skin friction and Nusselt number with varies parameters effects and constant parameters $\varphi_1 = 0.01, \varphi_2 = 0.02, S = 2.0, Pr\ Pr = 6.2, si = 0.1, K = 0.05$. ([] is second solution).

α	GO	R	β	a, b	γ	$Re^{1/2}{}_x\, C_f$	$Re_x{}^{-1/2}\, Nu_x$
-2.5	0	0.2	0.01	0.1	0.02	7.31915349 [0.32118018]	9.11990658 [5.69395518]
	0.01					7.33108631 [0.37396419]	9.07400085 [5.53374996]
	0.02					7.34115021 [0.42893614]	9.02429283 [5.37609791]
	0.03					7.34920523 [0.48624297]	8.97080069 [5.22250266]
	0.02	0.4				7.82690058 [0.1507408]	9.0551083 [0.81270981]
		0.6				8.27164481 [-0.08489143]	9.08199203 [-10.9586209]
		0.8				8.68515738 [-0.28763539]	9.10597754 [-32.0660575]
		0.2	0			7.81022231 [0.15432498]	9.01269891 [0.87364914]
			0.05			7.77531651 [0.13796653]	9.20910612 [0.58865095]
			0.1			7.52621802 [0.12480965]	9.36840974 [0.34605371]

0.05	0.5		7.77531651 [0.13796653]	8.76372742 [15.8301005]
	1		7.77531649 [0.13796653]	8.16526678 [12.4141955]
	1.5		7.77531647 [0.13796653]	7.51490995 [11.1603616]
	0.5	0	7.77531651 [0.13796652]	10.3531999 [19.2536675]
		0.06	7.7753165 [0.13796653]	6.70496974 [11.6773231]
		0.1	7.77531648 [0.13796653]	5.42948561 [9.25057937]

Velocity and Temperature Profiles

It is worth noting that the GO nanoparticles will significantly giving impact on fluid velocity and temperature of the flow. Based on Fig. 2, the velocity profiles abatement as the GO concentrations amplified. This is due to the intensified of the fluid viscosity, density and the advancement of internal interplay between GO and the boundary layer which leads to increase the boundary layer thickness. The effect of GO also impact the temperature profile to maximise as per illustrated in Fig. 3. It is due to the fact that the thermal conductivity and heat capacity augmentation which causing to further enhance the thermal dispersion and also the radiative heat transferal.

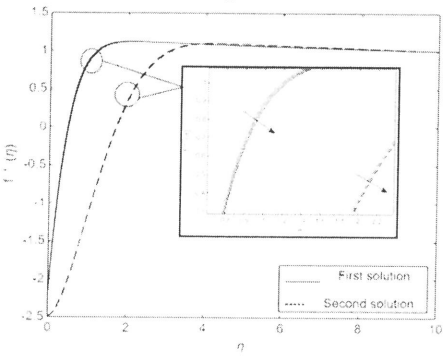

FIGURE 2. Velocity variation for several value of GO concentration φ_3 when $\lambda = -2.5, \varphi_1 = 0.01, \varphi_2 = 0.02, S = 2.0, Pr = 6.2, si = 0.1, Rd = 0.05$.

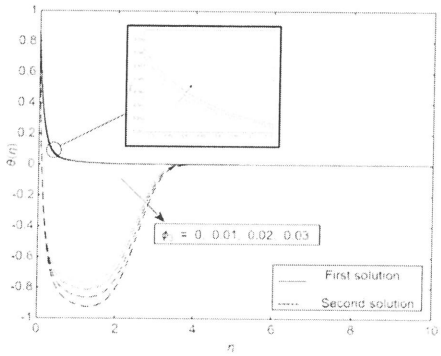

FIGURE 3. Temperature variation for several value of GO concentration φ_3 when $\lambda = -2.5, \varphi_1 = 0.01, \varphi_2 = 0.02, S = 2.0, Pr = 6.2, si = 0.1, Rd = 0.05$.

Figure 6 adorned the augmentation of velocity profile as velocity slip amplified. The physical reason behind this phenomenon is the shear stress at the surface decreases tagging along the viscous drag together. However, the temperature profile shown in Fig. 7 observed that a declination in temperature profile as the velocity slip growth. The slip growth enhances further the convective heat transferal which then subsidence the thermal boundary layer. Since the boundary layer is thinner, the heat dispersion is escalated through the fluid flow. It affected the heat removal which causing the reduction in surface temperature.

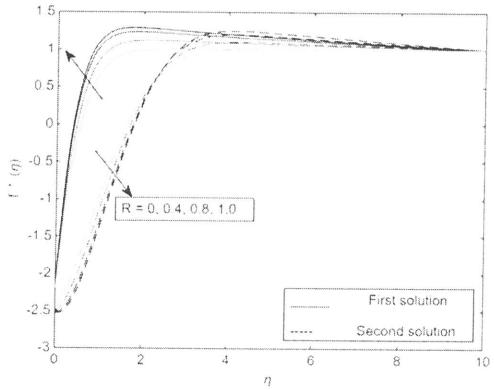

FIGURE 4. Velocity variation for several value of EMHD parameter R when $\lambda = -2.5, \varphi_1 = 0.01, \varphi_2 = 0.02, S = 2.0, Pr = 6.2, si = 0.1, Rd = 0.05$.

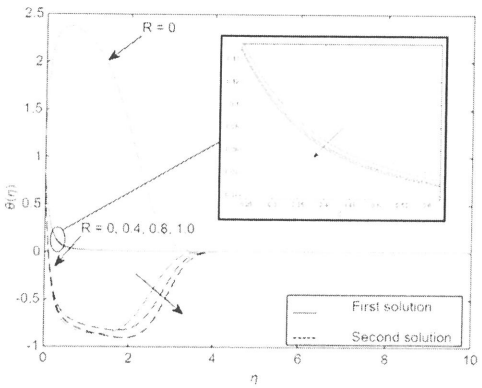

FIGURE 5. Temperature variation for several value of EMHD parameter R when $\lambda = -2.5, \varphi_1 = 0.01, \varphi_2 = 0.02, S = 2.0, Pr = 6.2, si = 0.1, Rd = 0.05$.

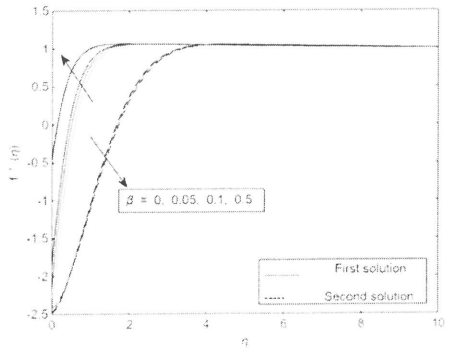

FIGURE 6. Velocity variation for several value of velocity slip β when $\lambda = -2.5, \varphi_1 = 0.01, \varphi_2 = 0.02, S = 2.0, Pr = 6.2, si = 0.1, Rd = 0.05$.

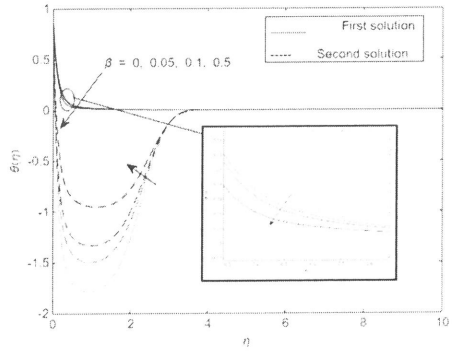

FIGURE 7. Temperature variation for several value of velocity slip β when $\lambda = -2.5, \varphi_1 = 0.01, \varphi_2 = 0.02, S = 2.0, Pr = 6.2, si = 0.1, Rd = 0.05$.

The temperature profile pictured in Fig. 8 shows the inflation as the non-uniform heat source amplified due to the intense heating will causing hot area which will improving the gradient of the thermal as well as hike the temperature of the flow. All effects such as thermal energy, patterns of the flow and interaction with the surface contributed to upturn the temperature profile. Conversely, the effect of non-uniform heat sink pictured in Fig. 9 illustrates that the temperature profile dwindling due to the heat removal from the fluid flow with enhanced thermal gradients in the system thus, the temperature shrinkage. The non-uniform heat sink modified the pattern flows and impacted the boundary layer to cool down.

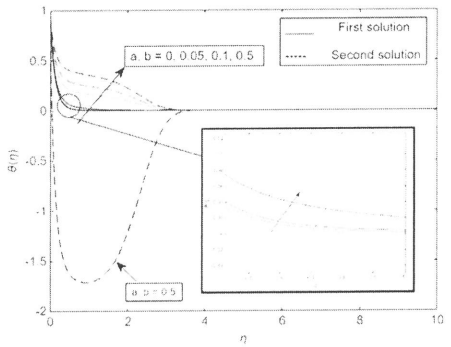

FIGURE 8. Temperature variation for several value of non-uniform heat source a, b when $\lambda = -2.5, \varphi_1 = 0.01, \varphi_2 = 0.02, S = 2.0, Pr = 6.2, si = 0.1, Rd = 0.05$.

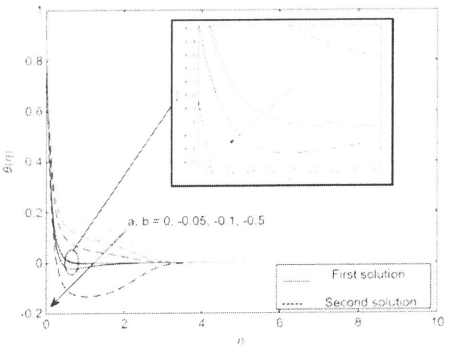

FIGURE 9. Temperature variation for several value of non-uniform heat sink a, b when $\lambda = -2.5, \varphi_1 = 0.01, \varphi_2 = 0.02, S = 2.0, Pr = 6.2, si = 0.1, Rd = 0.05$.

Figure 10 indicates that the thermal slip diminution the temperature profile because of the thermal resistance shrinkage and further upsurge the heat loss in the flow. The thermal slip also creates a steeper gradients of the temperature neighbouring boundary layer as well as the energy balance being altered within the fluid flow. The combination of boosting the convective cooling and alteration of flow dynamics contributed to declining temperature profile.

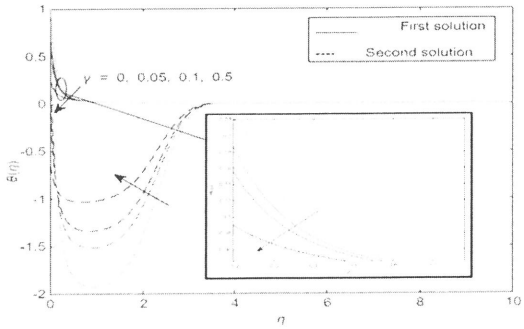

FIGURE 10. Temperature variation for several value of thermal slip γ when $\lambda = -2.5, \varphi_1 = 0.01, \varphi_2 = 0.02, S = 2.0, Pr = 6.2, si = 0.1, Rd = 0.05$.

CONCLUSION

The mathematical model of EMHD ternary hybrid nanofluid flow and heat transfer over shrinking Riga plate with several effects are constructed. The model is then being solved using bvp4c solver and the validation have been pointed out to prove the solutions are reliable. Based on the findings, the skin friction is escalating as the GO concentration and EMHD parameter upsurge but will decline as velocity slip hiked. The Nusselt number also augmented as GO concentration, EMHD and velocity slip amplified but diminished as the thermal slip and non-uniform heat source increases. Furthermore, the velocity profile is upturn as EMHD and velocity slip amplified, nonetheless the velocity profile subsidence as GO concentrations increased. While the temperature profile increment with GO concentrations and non-uniform heat source upsurged, only then the temperature profile is decreased with EMHD, non-uniform heat sink, velocity and thermal slip parameter.

ACKNOWLEDGEMENTS

The authors express their gratitude to the Ministry of Higher Education Malaysia, Universiti Putra Malaysia, and National Defence University of Malaysia for their valuable supports in facilitating this study. This research was funded by Universiti Putra Malaysia, grant number GP-IPM 9787700.

REFERENCES

1. S. Nasir, A. Berrouk, and Z. Khan, Appl. Therm. Eng. **242**, 122531 (2024).
2. M. Abbas, N. Khan, M. S. Hashmi, F. M. Tawfiq, S. Rezapour, M. Bilal, and M. Inc, Case Stud. Therm. Eng. **59**, 104546 (2024).
3. T. Sajid, A. A. Gari, W. Jamshed, M. R. Eid, N. Islam, K. Irshad, G. C. Altamirano, and S. M. El Din, Case Stud. Therm. Eng. **47**, 103058 (2023).
4. S. Jakeer, S. R. R. Reddy, A. M. Rashad, M. L. Rupa, and C. Manjula, Forces Mech. **10**, 100177 (2023).
5. M. I. Afridi, C. S. Reddy, A. R. Deepika, and K. Govardhan, Case Stud. Therm. Eng. **60**, 104783 (2024).
6. K. Ur Rehman, W. Shatanawi, and A. B. Colak, Case Stud. Therm. Eng. **54**, 103995 (2024).
7. T. Thumma and S. R. Mishra, J. Comput. Des. Eng. **7(4)**, 412 – 426 (2020).
8. S. A. Khan, T. Hayat, and A. Alsaedi, Case Stud. Therm. Eng. **54**, 104074 (2024).
9. S. Al Arni, A. El Jery, Z. Ullah, M. D. Alsulami, E. R. El-Zahar, L. F. Seddek, and N. B. Khedher, Case Stud. Therm. Eng. **60**, 104681 (2024).
10. Z. Mahmood, K. Rafique, U. Khan, T. Muhammad, Adnan, T. Alballa, H. A. E. and Khalifa, Mater. Today Commun. **40**, 109664 (2024).
11. M. Z. H. Supian, N. A. A. M. Nasir, and A. Ishak, Magnetohydrodynamics **57(3)**, 405 – 416 (2021).
12. N. A. Aminuddin, N. A. A. M. Nasir, W. Jamshed, N. Abdullah, A. Ishak, I. Pop, and M. Eid, Ain Shams Eng. J. **15(4)**, 102648 (2024).
13. E. M. Abo-Eldahab and M. A. El Aziz, Int. J. Therm Sci. **43(7)**, 709 – 719 (2004).
14. M. Muhammad, S. Islam, H. Ullah, and Z. Shah. J. Mol. Liq. **390(B)**, 123179 (2023).
15. N. Zainuddin, N. A. A. M Nasir, N. Abdullah, W. Jamshed, and A. Ishak, J. Adv. Res. Fluid Mech. Therm. Sci. **112(1)**, 62–75 (2023).
16. N. A. A. M. Nasir, N. Zainuddin, N. S. Khashi'ie, A. Ishak, and I. Pop, "Influence of Induced Magnetic Over Stagnation Point Ag-MgO/H_2O Hybrid Nanofluid Flow and Heat Transfer Towards Moving Surface," in *Intelligent Systems Modeling and Simulation II. Studies in Systems, Decision and Control*, edited by S. A. Abdul Karim (Springer, Cham, 2022), pp 447–465.
17. S. Swain, G. M. Sarkar, and B. Sahoo, J. Comput Sci-Neth **75**, 102207 (2024).
18. A. A. A. Arani and H. Aberoumand, Powder Technol. **380**, 152 – 163 (2021).